Fiber Optic Pulsed Polarimetry Measurements of DIII-D Poloidal Field[a)]

W. D. Kimura,[1,b)] D. S. Dhillon,[1] S. Munaretto,[2] E. J. Strait,[2] D. Du,[2] S. Loranger,[3] J-S. Boisvert,[3] and R. Kashyap[3]

[1]*STI Optronics, Redmond, Washington 98052, USA*
[2]*General Atomics, San Diego, California 92186, USA*
[3]*Department of Engineering Physics and Department of Electrical Engineering, Polytechnique Montreal, Montreal H3C 3A7, Canada*

(Presented XXXXX; received XXXXX; accepted XXXXX; published online XXXXX)

A new technique for measuring the spatial and temporal structure of the poloidal field is presented, in which the magnetic field causes the polarization of light traveling through an optical fiber to rotate via the Faraday effect by an amount proportional to the strength of the field oriented along the fiber. In fiber optic pulsed polarimetry, changes in the polarization of the backscatter light from the fiber are detected, thereby permitting measurement of the field as a function of position along the fiber. In this proof-of-principle experiment, specially prepared single-mode fibers with weak fiber Bragg gratings were installed in the poloidal direction on the outside of the thermal blanket on DIII-D. Light at 532 nm from a mode-locked Nd:YAG laser was injected into the optical fibers. The laser repetition rate was 895 kHz with a pulse length of <10 ps, resulting in ~1 μs temporal resolution. A photodetector system measured the Stokes polarization components necessary to determine the amount of polarization rotation. For this experiment, bandwidth limitations of the detectors resulted in a spatial resolution of ≈2 cm. The measured temporal and spatial distributions of the poloidal field are consistent with inductive probe measurements and EFIT reconstructions of the spatial distribution. This demonstrates the ability of this technique to provide real-time detection of the temporal and spatial variations of the poloidal field. Besides revealing more detailed information about the plasma, this new diagnostic capability can also help in detecting instabilities in real-time, thereby enabling enhanced machine protection.

I. INTRODUCTION

Measurement of the distributed magnetic fields on magnetic fusion energy (MFE) devices is critical to ensure confinement of the plasma through control of its shape and to diagnose the plasma. Precise measurements of the poloidal and radial component of the magnetic field at the vacuum vessel are important for reconstruction and control of the plasma magnetic equilibrium. Detailed high time resolution poloidal field profiles would enable detection of the onset of plasma instabilities, such as tearing modes and edge localized modes (ELMs).

Many diagnostics exist to measure the magnetic field, for instance Rogowski and pick-up coils. These are primarily inductive sensors and, as such, become less effective during quasi-steady-state conditions, which MFE devices are striving to achieve. They are susceptible to noise and drift problems, which can be aggravated by the need to have long electrical conductors in close proximity to high voltages. Radiation effects can degrade their electrical insulation. Their spatial resolution is also limited by the number of sensors that can be positioned around the MFE device. Installing many sensors becomes unwieldy as space must be found for all the sensors and additional sensing electronics must be installed.

Fiber optics to measure the magnetic field on MFE devices offer a paradigm shift away from these inductive sensors. These fibers utilize the Faraday effect in which the magnetic field rotates the polarization of light traveling through the fiber.[1] Fiber sensors have several advantages including resilience against electrical noise, no electrical hazard, and elimination of drift problems.

While fiber optics have been used to obtain spatially-integrated field measurements of MFE devices,[2] the approach described in this paper further extends this by enabling both temporal and spatial measurement of the field. The key to this new approach is sending ultrashort laser pulses (~10 ps) through the fiber and detecting the backscatter light. This permits measuring the magnetic field distribution with high spatial resolution (e.g., ~2 cm as limited by the detector/digitizer bandwidth/sampling rate). Moreover, by using a high-repetition rate laser (~1 MHz), the time variation of the field can also be measured with ~1-μs resolution. Thus, the system is able to provide this 2-D data (space and time) without the need to add additional sensing electronics for each data point. This dramatically increases the magnetic field detection coverage compared to using discrete electrical probes. This technique is called fiber optic pulsed polarimetry (FOPP). It is based upon work developed by R. J. Smith[3-4] in which

[a)]Published as part of the Proceedings of the 22nd Topical Conference on High-Temperature Plasma Diagnostics (HTPD 2018) in San Diego, California, USA.
[b)]Author to whom correspondence should be addressed: wkimura@stioptronics.com.

pulsed polarimetry of laser light propagating in free space can be used to probe the plasma characteristics.

A measurement of the poloidal field distribution outside of the magnetically confined plasma using the FOPP diagnostic would permit equilibrium reconstructions, sensing vertical instabilities, measuring the plasma equilibrium shape in greater detail than an array of pickup coils, and provide machine protection by way of feedback for non-axisymmetric saddle coils. Thus, this potential capability to quickly detect the onset of instabilities may be critical for being able to safely shut down the machine to prevent damage.

The laser drive source for the FOPP diagnostic can be located away from any radiation hazards. Different methods can be used for multiplexing the output of multiple fibers into the data acquisition system, thereby, minimizing the laser and detector costs. The optical bandwidth of fused silica fibers is essentially instantaneous; there is no saturation of the Faraday effect and no hysteresis. Fiber optic technology is well developed via its ubiquitous usage in the telecommunication industry.

II. DESCRIPTION OF FOPP TECHNIQUE

A linearly polarized laser beam traveling through a single-mode (SM) optical fiber will experience rotation of its polarization direction due to circular birefringence when a magnetic field is applied along the direction of the fiber. The amount of the angular rotation ψ is given by

$$\psi = V \oint H \cdot ds, \tag{1}$$

where V is the Verdet constant (Faraday magneto-optic constant), and the line integral over the magnetic field H is over the area defined by the closed optical fiber loop. The circular birefringence is a nonreciprocal effect, which means that the direction of rotation with respect to the fiber axis is the same regardless of the direction of the light traveling through the fiber. This fact doubles the amount of rotation for a given magnetic field strength when observing backscattered light.

The full characterization of the polarization state of the light can be expressed using the four Stokes parameters s_0 to s_3 associated with the Poincare Sphere given by

$$\begin{bmatrix} s_0 \\ s_1 \\ s_2 \\ s_3 \end{bmatrix} = \begin{bmatrix} I_{\text{total}} \\ \cos 2\chi \cos 2\psi \\ \cos 2\chi \sin 2\psi \\ \sin 2\chi \end{bmatrix}, \tag{2}$$

where I_{total} is the total intensity and χ is the ellipticity (elongation) angle for an elliptical representation of the polarization. The Stokes parameters can be determined by detecting the following polarization intensity components of the backscatter light: s-polarization ($I_{s\text{-pol}}$), p-polarization ($I_{p\text{-pol}}$), polarization oriented at 45° relative to the s-pol and p-pol ($I_{45\text{-deg}}$), and 45° polarization that also incorporates a quarter-wave plate ($I_{\lambda/4}$). Then, $s_0 = I_{s\text{-pol}} + I_{p\text{-pol}}$, $s_1 = I_{s\text{-pol}} - I_{p\text{-pol}}$, $s_2 = 2I_{45\text{-deg}} - s_0$, and $s_3 = 2I_{\lambda/4} - s_0$.

For determining ψ, it is only necessary to use the s_1 and s_2 components via[5]

$$\psi = \frac{1}{2}\tan^{-1}\left(\frac{s_2}{s_1}\right) = \frac{1}{2}\tan^{-1}\left(\frac{2I_{45\text{-deg}} - I_{s\text{-pol}} - I_{p\text{-pol}}}{I_{s\text{-pol}} - I_{p\text{-pol}}}\right), \tag{3}$$

To increase the intensity of the backscatter light to permit detection using fast avalanche photodiodes (APDs), R. J. Smith conceived the idea of imprinting low-reflectivity fiber Bragg gratings (FBGs) distributed at regular intervals along the fiber. Four SM fibers were imprinted by Polytechnique Montréal[6] with 0.2-mm-long FBGs spaced 1 cm apart over a 1-m length of the fiber. Each grating has a reflectivity at 532 nm of ≈0.2%. These specially modified fibers are referred to as backscatter-tailored fibers (BTFs). Since the gratings reflect light in either direction, the backscatter signal tends to be strong for the first gratings and then steadily decreases to near zero by the last gratings, which is why the sensing portions of the BTFs were limited to ~1 m. Longer lengths would be possible using a laser with higher operating characteristics than the one used here (see Sec. V).

III. DESCRIPTION OF EXPERIMENT

Figure 1 depicts the estimated positions of the BTFs on the thermal blanket of the DIII-D tokamak. Each BTF is drawn in a different color with the length of the colored segment representing the 1-m long FBG-imprinted sensing region along the fiber. BTF #1 and #3 sense the poloidal field near the mid-plane of the tokamak; BTF #2 and #4 sense the field near the top and bottom of the vessel. We should emphasize that as a proof-of-principle experiment operating parasitically, the options for placement of the fibers on DIII-D were very limited. The fibers were aligned in the poloidal direction on a best effort basis, but their exact positions could not be verified once they were inserted underneath the hardware located over the blanket.

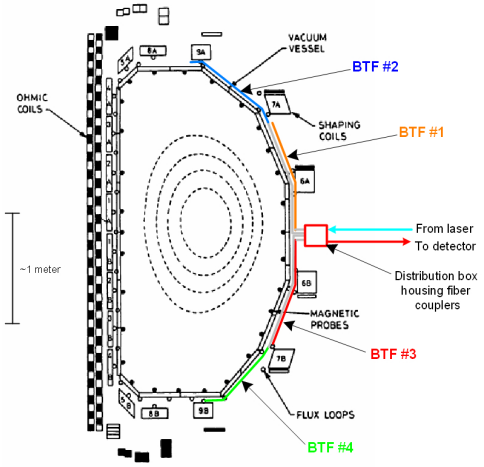

Fig. 1. Cross-sectional diagram of DIII-D vacuum vessel showing approximate location of optical fibers aligned along poloidal direction. BTFs are depicted in different colors where the length of the colored line segments represents approximately the 1-m length of the FBGs section. Gray-colored lines connected to the colored lines represent regular SM fibers connected to the BTFs with no gratings imprinted on them.

The mode-locked, 532-nm laser for driving the fibers is located in a separate room and produces a continuous train of <10 ps pulses at 895 kHz repetition rate. It delivers 82 μW into a 37-m SM fiber cable that extends from the laser to the distribution box located next to the DIII-D tokamak (see Fig. 1). This amount of power is sufficient to generate adequate backscatter signals from pairs of BTFs. Hence, during a plasma shot, the poloidal field was measured either by BTF #1 and #2, or BTF #3 and #4. A 2×2 fiber coupler inside the distribution box combines the backscatter signal from the pair of BTFs into a single fiber cable where the extra-long lengths of BTF #2 and #4 were designed so that their backscatter signals are passively delayed in time relative to BTF #1 and #3, respectively. This means the backscatter signal sensed by the photodetectors consists of the first BTF followed immediately in time by the second BTF. This illustrates how multiplexing the fibers enables creating an effective 2-m long sensing region using two 1-m BTFs. This cable extends to the photodetector system located ≈5 m away from the tokamak. Three APDs (2.3 GHz) with built-in transimpedance amplifiers sense the *s*-pol, *p*-pol, and 45-deg signals. In order to maintain isolation of the electrical ground of the tokamak, the RF outputs from the APDs are connected to fiber-optic data transmitters (3 GHz bandwidth) whose fiber optic cables bring the APDs signals back to the room housing the laser system. Fiber-optic data receivers convert the signals back to RF ones and high-speed digitizers (2.5 GHz bandwidth, 5 GS/s sampling) are used to capture the backscatter signals.

Due to various birefringence effects not related to the presence of the magnetic field, the backscatter light from each BTF displays a static polarization distribution along each fiber. When a magnetic field occurs along the fiber, it will change this polarization distribution; hence, it is the net change in polarization angle from the static case that is of interest. This net change can be determined by having the first acquisition, which is obtained just before the shot commences, serve as the reference static polarization state for each BTF. The reference polarization angle distribution is subtracted from the polarization angle distributions for each of the acquisitions to yield the net change in angle $\Delta\psi$. The poloidal field is then given by $B_{\text{pol}} = \Delta\psi/2VL$, where for fused silica $V \approx 270°$/m-T, L is the length of the fiber exposed to the B-field, and the factor of 2 accounts for the light double-passing through the fiber.

IV. EXPERIMENTAL RESULTS

Since a continuous train of backscatter signals are being generated, the digitizers are set to acquire a preselected number of backscatter pulses (e.g, 50-120) at preselected time intervals (e.g., 100-150 ms) shortly before and during the plasma shot for a preselected number of acquisitions (e.g., 70-90). Savitzky-Golay filtering and averaging over the 50-120 backscatter light pulses is applied to reduce the noise level and yield a single backscatter profile for each polarization component for each acquisition. These polarization values are entered into Eq. 3 to calculate ψ as a function of position along the fiber. Thus, each acquisition shows the spatial distribution of the poloidal field along a pair of fibers while the series of acquisitions shows the time dependence of the poloidal field.

Shown next is an example of the FOPP results compared with predicted measurements based on the EFIT[7] equilibrium reconstruction from flux loop, Mirnov, and Rogowski coil data.[8] Figure 2 gives the color-coded EFIT Bz and Br reconstructions for Shot 173919 at t = 3.66 s derived from the 65×65 EFIT output matrix. Overlaid on the 2D plots is the approximate location of the fibers on the outside of the tokamak where BTF#1 and #2 are in the upper half, based on the location of the flux loops (white dots).

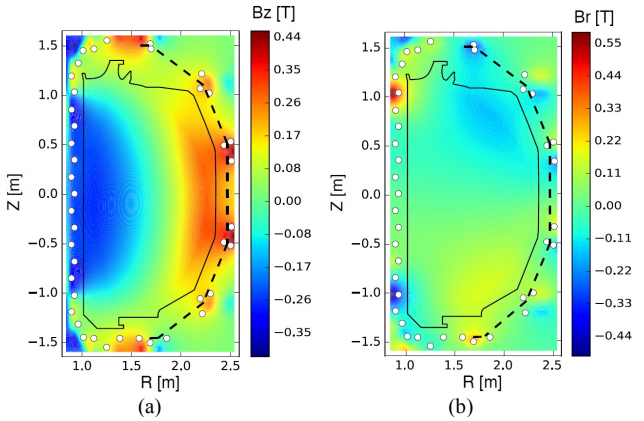

(a) (b)

Fig. 2. EFIT reconstruction of poloidal field for Shot 173919. Approximate position of fibers shown as black dashed lines. (a) Bz (vertical) field. (b) Br (horizontal) field.

Figure 3 shows the FOPP results for Shot 173919 at t = 3.66 s obtained from BTF#1 and #2, where the BTF#1 results extend from approximately 0-1 m and the BTF#2 results are from about 1-2 m. Also plotted is the predicted field from the equilibrium reconstruction where the field component along the fiber direction is calculated by combining the appropriate projections of the Bz and Br components at each position along the fiber. Since the exact positions of the fibers on the EFIT plots in Fig. 2 are uncertain, the error bars represent how much the field varies in the plot on either side of the dashed line in Fig. 2.

Although there is a difference in the absolute magnitude of the field between the FOPP data and the EFIT reconstructions, there is consistency in the overall spatial distribution pattern displayed. Indeed, examining Fig. 2, we see that EFIT shows pockets of higher field that give rise to the peaks seen in Fig. 3. The FOPP data also shows peaks in similar locations. The exception is near the end of BTF#2, which does not display as pronounced a peak as the EFIT reconstruction. Note, however, at this location that the EFIT reconstruction has a wide variation for small changes in location within its matrix. Thus, it is possible the true position of the end of BTF#2 may be located farther away from the sharp peak region reconstructed by EFIT at this spot. This is plausible

because the exact position of the end of BTF#2 could not be visually confirmed.

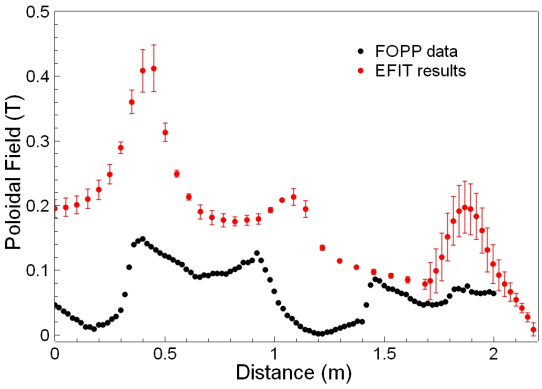

Fig. 3. FOPP results for Shot 173919 at t = 3.66 s along with the EFIT reconstruction where the error bars represent the uncertainty of the fiber position relative to the EFIT results shown in Fig. 2.

Figure 4 shows the poloidal field measured for Shot 173944 using BTF#3 and #4 at various times where t = 0 corresponds to the nominal start of plasma formation. We see there is no appreciable field at t = -2.435 s [Fig. 4(a)], then the field begins to grow and reaches a quasi-steady state after several seconds [Figs. 4(c) and 4(d)].

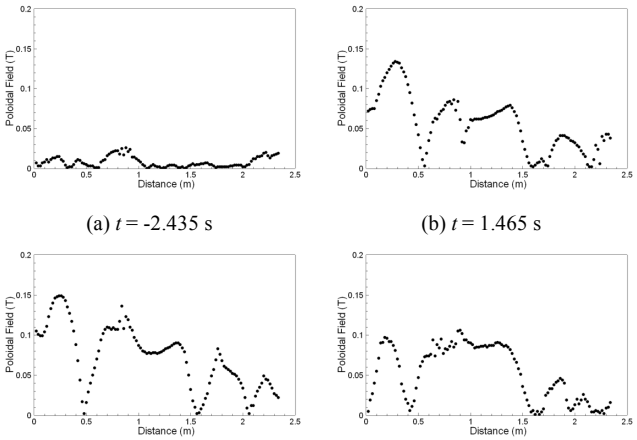

(a) t = -2.435 s (b) t = 1.465 s

(c) t = 2.965 s (d) t = 4.765 s

Fig. 4. FOPP results for Shot 173944 at various times during plasma shot.

The time dependence of the field as measured by the fibers is displayed in Fig. 5 for Shot 173944, in which the field at one position along each fiber is plotted versus time. Also plotted are time traces of the magnetic field measured by inductive probes located inside the tokamak.[8] The inductive probes, mpi6fb322 and mpi79b322, are roughly at the same azimuthal position as the centers of BTF #3 and #4, respectively. The inductive probes are located at 322° toroidally, which were the closest ones to the fibers located at 135°. Except for small variations ($\delta B/B \leq 10^{-4}$), the magnetic field is expected to be toroidally symmetric.

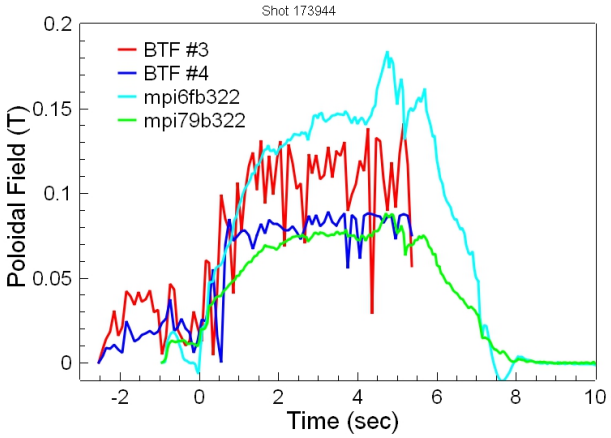

Fig. 5. Comparison of poloidal field time dependence results between FOPP data and inductive probes for Shot 173944. Inductive probes mpi6fb322 and mpi79b322 are approximately at the same azimuthal position as the centers of BTF #3 and #4, respectively. However, the inductive probes are located at 322° toroidally; whereas, the fibers are located at 135°.

In Fig. 5, we see both the inductive probes and the FOPP data display small amounts of signals before t = 0, and then both the probes and data begin rising and reaching plateaus at roughly the same time. The magnitude of the field measured by BTF #4 is comparable to mpi79b322; whereas, the magnitude of the field from BTF #3 is less than mpi6fb322. These magnitude differences may be due to the fibers being located farther away from the plasma than the inductive probes.

The FOPP data appears noisier than the inductive probes; however, this degree of noise is not observed when examining the raw polarization data where only gradual changes in the shapes of the polarization plots are evident during the plasma shot. It appears that a significant portion of this noise is introduced during the data reduction process. The three polarization components must be aligned accurately in time, but due to various noise sources, such as from the fiber-optic data transmitters, there can be still residual temporal misalignment between adjacent acquisitions. Equation 3 is particularly sensitive to regions where the s-pol and p-pol profiles cross each other since the denominator of the argument in Eq. 3 is the difference between these components. Therefore, small temporal shifts between the components can cause large variations in ψ.

To confirm the fibers were not detecting other magnetic fields components, e.g., toroidal, two tests were performed. The first was having the data acquisition system perform a normal capture of the backscatter light without the tokamak firing. No change in the polarization was detected for all the acquisitions. The second test was capturing the backscatter light when the tokamak was fired, but with no plasma. The fibers detected no appreciable signal; whereas, the inductive probe showed a small signal. This implies the fibers are not detecting any significant signal from the toroidal field.

There are several possible reasons for the differences between the FOPP and the probe/reconstruction results

seen in Figs. 3 and 5. As mentioned, the nature of this experiment precluded accurately positioning the fibers, which complicates the ability to precisely compare with the probes and reconstructions. The actual value for the Verdet constant is uncertain; a generic one for fused silica was assumed. The true value may be smaller, which is plausible given that the fibers are not pure SiO_2. This might help explain the magnitude differences, especially in Fig. 3. The position along the fiber of the backscatter signal depends on knowing precisely the effective index of refraction of the fiber. Again, a generic value for the index was assumed, but the true value may change this distance, thereby altering the width of the data in Fig. 3. Clearly, additional FOPP experiments are needed where the BTFs have been precisely aligned, and their Verdet constant and refractive index measured independently.

V. DISCUSSION

As a proof-of-principle experiment, its aim was to demonstrate that the FOPP technique is capable of detecting the relatively weak poloidal field, which tends to be an order of magnitude smaller than the toroidal field. The fact it achieved this with only 41 μW of laser power feeding into each BTF attests to the high sensitivity of this technique. Nevertheless, to apply this technique for diagnosing the entire surface area around the tokamak will require driving many long lengths of fiber.

There are several ways the FOPP technique can be improved to permit scaling it up. First, the particular laser used was convenient for this experiment, but not optimum for a dedicated diagnostic system. Using lasers operating at 1.06 μm wavelength, where the APDs are more sensitive, and at longer pulse lengths (e.g., ~100 ps) will greatly increase the backscatter signal while still providing adequate spatial resolution. If 1-μs time resolution is not needed, then powerful, lower repetition rate lasers are available that would be able to drive many multiplexed fibers simultaneously.

A stronger backscatter signal has other advantages. It allows sending the signal via fiber optic cables directly back to the photodetectors located farther away from the tokamak, thereby eliminating noise sources, such as the fiber-optic data transmitters/receivers.

Second, high-bandwidth APDs generally have very small detector areas that require tight focusing of the backscatter light onto the detector area. Hence, utilizing a more sophisticated focusing arrangement than used during this experiment would significantly increase the APD signal. Higher bandwidth, higher sampling rate digitizers are also available, which would improve the resolution of the measurement system, thereby facilitating the data reduction process.

Third, the SM fibers used to make the BTFs were standard, commercially available fibers. As mentioned, their Verdet constants may be on the low side. Fibers made from SF-57 glass and Tb-doped fibers[9] have much higher Verdet constants, which would substantially increase the sensitivity of this diagnostic.

Fourth, the fibers for this experiment were limited where they could be positioned on DIII-D due to the lack of unobstructed space on the outside of the machine. They also had to be installed over the thermal blanket. In a dedicated system, since the fibers can be designed to withstand bake-out temperatures, the fibers could be installed under the thermal blanket, or it is conceivable that bare fibers could be installed inside the tokamak behind the tiles. These options would position the fibers closer to the plasma, thereby increasing their signal strength.

Lastly, refinement of the data reduction process can be performed, in particular, improving the calculation of the amount of polarization rotation from the polarization components to minimize introducing noise. The reduction process can be fully automated to permit real-time monitoring of the magnetic field distribution over the entire fiber optic network covering the device.

As an aside, we should mention that ITER has already investigated the effects of radiation on optical fibers and shown it does not change the Verdet constant.[10] Various approaches are possible for handling radiation darkening, including taking advantage of the bake-out to intentionally heat the fibers in order to anneal out the darkening.

V. CONCLUSION

This experiment demonstrated the ability of the FOPP diagnostic to provide both high-resolution spatial and temporal measurements of the DIII-D poloidal field. Its results are consistent with inductive probe measurements and equilibrium reconstructions of the poloidal field. This opens up the possibility of using this new diagnostic to improve measuring the plasma characteristics and provide real-time monitoring to enhance machine safety.

VI. ACKNOWLEDGMENTS

We wish to acknowledge Rejean Boivin, Thomas Carlstrom, Fenton Glass, Matt Watkins, James Kulchar, Federico Halpern, and Brian Petrich for their assistance during the performance of this experiment. This work was supported by US DOE under Grant Nos. DE-SC0009808 and DE-FC02-04ER54698.

[1]A. J. Rogers, Appl. Optics **20**, 1060-1074 (1981).
[2]Ph. Moreau, B. Brichard, A. Fil, Ph. Malard, P. Pastor, A Le-Luyer, F. Samaille, and V. Massaut, Fusion Eng. Design **86**, 1222-1226 (2011).
[3]R. J. Smith, Rev. Sci. Instrum., **79**, 10E703 (2008).
[4]R. J. Smith, 14th Laser Aided Plasma Diagnostics Conference, Treviso, Italy, (2009).
[5]D. H. Goldstein, *Polarized Light, 3rd Ed.* (CRC Press, Boca Raton, FL, 2011).
[6] M. Gagne, L. Bojor, R. Maciejko, and R. Kashyap, Opt. Exp. 16, 21550 (2008).
[7]L. L. Lao, J. R. Ferron, R. J. Groebner, W. Howl, H. St. John, E. J. Strait, and T. S. Taylor, Nucl. Fusion **30**, 1035 (1990).
[8]E. J. Strait, Rev. Sci. Instrum. **77**, 023502 (2006).
[9]L. Sun, S. Jiang, and J. R. Marciante, Optics Exp. **18**, 5407 (2010).
[10]G. Vayakis, A. Gusarov, W. Leysen, ITER_D_64HX2L v1.0, 03-Jul-2011 (unpublished).

DISCLAIMER